



OPEN

Electrochemical etching strategy for shaping monolithic 3D structures from 4H-SiC wafers

André Hochreiter¹ , Fabian Groß, Morris-Niklas Möller, Michael Krieger¹ & Heiko B. Weber¹  

Silicon Carbide (SiC) is an outstanding material, not only for electronic applications, but also for projected functionalities in the realm of spin-based quantum technologies, nano-mechanical resonators and photonics-on-a-chip. For shaping 3D structures out of SiC wafers, predominantly dry-etching techniques are used. SiC is nearly inert with respect to wet etching, occasionally photoelectrochemical etching strategies have been applied. Here, we propose an electrochemical etching strategy that solely relies on defining etchable volumina by implantation of p-dopants. Together with the inertness of the n-doped regions, very sharp etching contrasts can be achieved. We present devices as different as monolithic cantilevers, disk-shaped optical resonators and membranes etched out of a single crystal wafer. The high quality of the resulting surfaces can even be enhanced by thermal treatment, with shape-stable devices up to and even beyond 1550°C. The versatility of our approach paves the way for new functionalities on SiC as high-performance multi-functional wafer platform.

Silicon Carbide (SiC), especially its polytype 4H-SiC, is an extraordinary material for integrating electronics¹, photonics², high-quality mechanics³ and quantum technologies on the very same chip^{4,5}. Due to its technological breakthrough in power electronics, it is available as single crystalline high-quality wafers. When, further, optical and mechanical functionality is demanded, there is a need for highest-quality devices with three-dimensional geometries. As to optics, SiC provides the unusual opportunity of simultaneous $\chi^{(2)}$ and $\chi^{(3)}$ nonlinearities^{6,7}. The current state-of-the-art photonics-on-a-chip is not integrated with traditional SiC fabrication techniques, but uses thin SiC-on-insulator technology^{4,8,9}. As to mechanics-on-a-chip, SiC provides an outstanding intrinsic property: it has the lowest internal damping of all known materials^{3,9,10}. Also here, device fabrication utilizes thin SiC layers on a sacrificial substrate. Given the extraordinary set of parameters of SiC, it is desirable to identify *monolithic* technologies for the preparation of optical and mechanical devices along with the electronic functionality. Compatibility with high-temperature protocols, for example epitaxial graphene growth¹¹ or defect annealing¹², would be beneficial.

For such applications, however, a technological prerequisite is an etching strategy that forms the desired 3D-structures monolithically out of the single-crystal wafer, while maintaining high-quality surfaces and low defect budgets. The commonly used gas etching strategies (ICP-RIE/RIE) are projective, and even ‘anisotropic’ gas etching has limited aspect ratios^{13–15}. Further, they are prone to create surface-near point-defects. Therefore, a new process strategy is required. In an effort to increase the design space for advanced 3D geometries like cantilevers, disk-shaped resonators or membranes (cf. Fig. 1), including long-range lateral etching, we present a route based on implantation and subsequent electrochemical etching (ECE).

SiC is nearly inert and only few chemical reagents to resolve it under moderate conditions are known. Typically, both high temperatures and strong etchants are needed¹⁶. Here we choose positive charge carriers (holes, h^+) at the surface for the electrochemical attack. We opt for etching under alkaline conditions, the electrochemistry of which has extensively been studied by *van Dorp*^{17–19}. In order to provide the required h^+ on the surface, a vast majority of publications uses electron–hole creation by ultraviolet light including our own previous work^{5,20–22}. This methodology is limited because of optical constraints, in particular it has poor vertical control²². Here we favor an electrochemical strategy where h^+ -concentrations are created by appropriate doping patterns. Additional control can be gained by electric potentials. In a late stage of our investigations, we found that the etching strategy is similar to²³.

Department of Physics, Friedrich-Alexander-Universität Erlangen-Nürnberg (FAU), 91058 Erlangen, Germany.
✉email: heiko.weber@fau.de

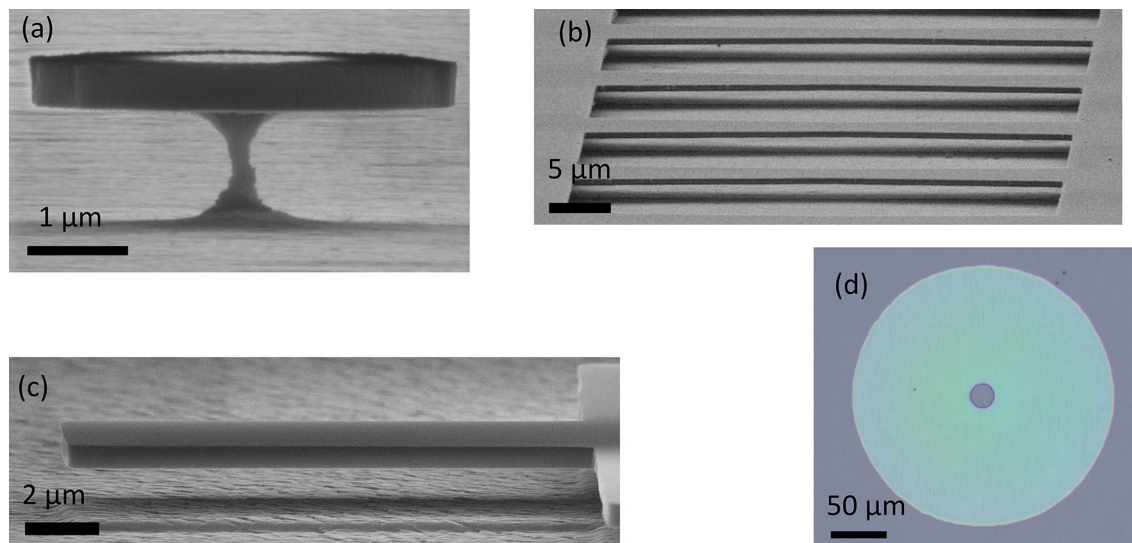
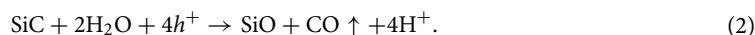
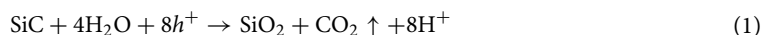


Figure 1. Monolithically etched 3D-devices from single-crystal 4H-SiC wafer. (a) disk-shape optical resonator, (b) doubly clamped mechanical resonator, (c) single clamped mechanical resonator, (d) free-standing circular membrane (central hole is required as etching access). (a–c) SEM micrographs, (d) optical micrograph.

Etching of SiC involves a two-step process. First, oxidation of SiC follows two possible reaction pathways for the oxidation²⁴:



According to current knowledge, both oxidation pathways take place simultaneously, while the applied voltage determines the ratio of both²⁵. Experimentally it is indeed reported that the dissolution valence, i.e. the number of charge carriers required to etch one formula unit of SiC is between 6 and 6.9^{18,24}. In a second step, the resulting reaction products SiO_x are removed by the electrolyte, that is potassium hydroxide (KOH). The dissolution of SiO_2 involves the adsorption of water with the formation of hydrated silica ($\text{SiO}_2 + 2\text{H}_2\text{O} \rightarrow \text{Si}(\text{OH})_4$) and an attack by hydroxyl ions to form a soluble silicate ($\text{Si}(\text{OH})_4 + 2\text{OH}^- \rightarrow [\text{Si}(\text{OH})_2\text{O}_2]^{2-} + 2\text{H}_2\text{O}$)^{26,27}.

In steady state, the oxidation of SiC and the subsequent dissolution of SiO_x occur with the same rate, which is our desired regime of operation, see Fig. 2. Otherwise, an overshooting of the SiO_2 -formation would passivate the surface and block the electrochemical process. This would result in an oscillatory behavior at higher rates, which we avoided by sticking to low reaction rates^{28,29}.

This electrochemical reaction gives a handle to remove specific volumina selectively. p-doped, i.e. h^+ -rich regions can efficiently be etched as opposed to n-doped regions where, due to the lack of h^+ , etching is completely suppressed.

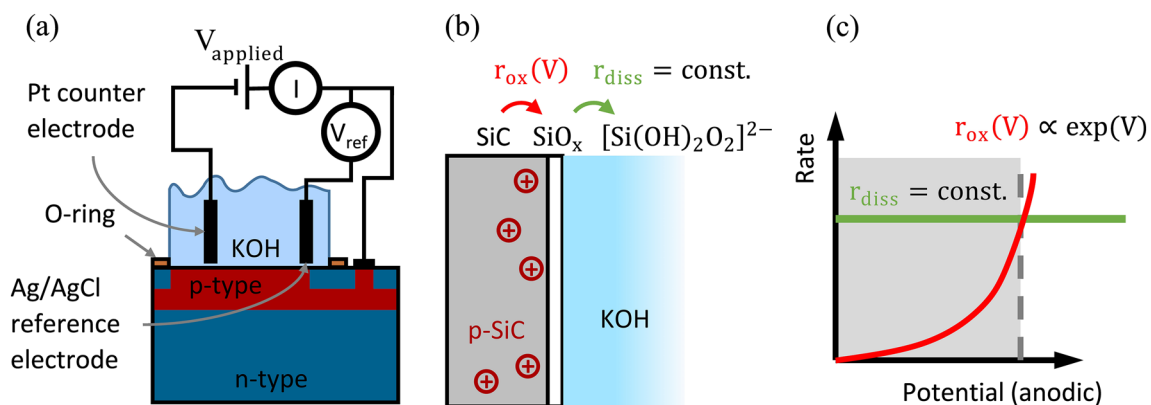


Figure 2. Electrochemical oxidation reactions. (a) Electrochemical etching setup. The current (I) flows via the p-SiC layer to the counter electrode. (b) Dissolution of SiC, forming SiO and SiO_2 as intermediates, subsequently forming soluble silicates. (c) Oxidation (r_{ox}) and dissolution (r_{diss}) rates as a function of applied voltage. The grey area indicates the voltage range suitable for steady-state etching.

We start with a 4°-off-axis n-type wafer with an epilayer (nitrogen-doped 10^{16} cm^{-3}). The required doping profiles can be defined by ion implantation, which is described in detail in the SI, detailed data can be found in³⁰. The hole concentration profile is shown in Fig. 3, where Aluminum-implantation creates a box-like p-type profile in a depth from 550 nm to 1.6 μm . At its flank, the hole concentration drops by more than ten orders of magnitude within 50 nm, which gives hope that the etch-stop is defined within atomic precision. In order to ensure reliable n-doping of the top layer, a counter implantation with Nitrogen is performed. Subsequent annealing to 1700°C for 30 min in 900 mbar Argon-atmosphere re-establishes the crystalline lattice (locally, a carbon cap stabilizes the surface³¹). Note that dopant diffusion is essentially absent in the rigid SiC-lattice.

For the geometries in this manuscript, we used only vertical implantation profiles. The methodology can be readily extended to more complex 3D structures, when in addition, lateral patterning of the implantation is achieved, for example with robust metallic masks.

But also with laterally homogeneous doping profiles, 3D structures can be defined. For this purpose, we pattern resist masks which define a top window (electron beam lithography or similar). A projective etching of the n-type layer is performed by standard RIE / ICP-RIE techniques, such that the p-SiC layer is slightly etched. Now, the ECE is performed, which isotropically removes the p-SiC layer, see Fig. 4. A typical lateral etch velocity is 2 $\mu\text{m}/\text{h}$. Care has to be taken that during this process an uninterrupted current path through the p-type layer has to be maintained. If however, p-type areas are disconnected from the current pathway during the etching, the dissolution stops for this island. While this may occur unintentionally, this property can also be exploited for the positive (see e.g. self-limited support columns for disk-shape optical resonators in Fig. 4). In any case, maintaining intact current pathways throughout the etching process has the rank of a design principle.

Figure 1 displays a cantilever-like structure after ECE. We report one complication that arises after the ECE. Underneath the top n-type layer, in barely accessible regions, often an undesired porous p-type structure remains (goat beard), see SI. It reminds the formation of porous SiC in KOH³⁵. It can reliably be removed by two simple techniques: either a subsequent isotropic dry etch with CF_4 at 190 mTorr that is suited for well-accessible devices like cantilevers, see SI. Alternatively, high temperature annealing beyond 1000°C in 900 mbar Argon atmosphere removes this layer even in hardly accessible regions. It can be suspected that thermal oxidation has a similar effect^{36,37}.

An obvious quality criterion for optical or mechanical devices is the surface roughness. In our devices, the ECE process leaves the etched surface quite smooth. The top surface of the n-SiC layer is essentially unchanged (in our experiments, $\text{rms}_{\text{top}} = 1.46 \text{ nm}$, see Fig. 5a). For characterizing the bottom layer, we removed a single clamped cantilever with scotch tape and studied its surface with the AFM. The result is shown in Fig. 5b, it yields $\text{rms}_{\text{bottom}} = 2.48 \text{ nm}$. Hence, both the unetched top and the freshly etched bottom surfaces have both low surface roughness.

Finally, we address the question, how the presented 3D fabrication technique is compliant with further processing. Underetched devices were spin-coated with PMMA and nLoF resist materials without being damaged. They also survived lift-off processes, rinsing and drying without special precautions. Remarkably, the devices are also robust with respect to high-temperature steps. In SiC, relevant spin-carrying color centers are created, converted and finally annealed out in a temperature range from 400°C to 1400°C¹². The native oxide layer sublimates at temperatures above 800°C in UHV³⁸. Epitaxial graphene fabrication in n-type 4H-SiC is performed at above 1500°C³⁹. Unintentional implantation damage anneals out at 1600°C to 1700°C. Hence, we explored this

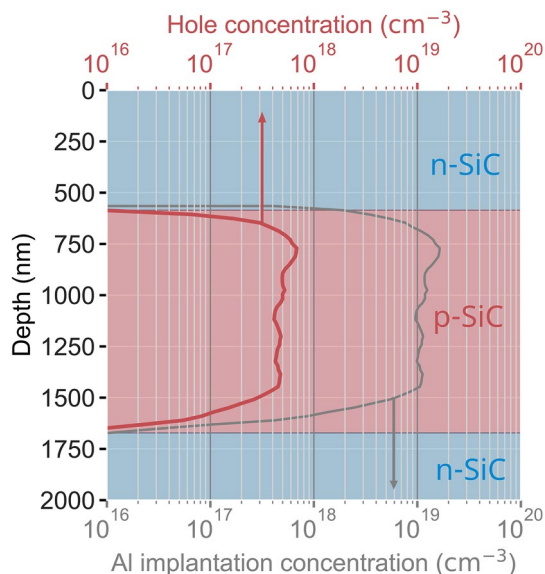


Figure 3. Dopant-defined layers for electrochemical etching. By suitable implantation profiles for Aluminum and Nitrogen, a sharply defined p-SiC layer with an excess of positive charge carriers (holes) is defined. The hole concentration is calculated, utilizing the charge neutrality equation, assuming a compensation ratio of 0.35³², and a doping concentration dependant ionization energy ($E_{\text{ion}}(N_{\text{Al}}) = 210\text{meV} - 3 \cdot 10^{-8} \text{ eVcm} \cdot N_{\text{Al}}^{1/3}$)^{33,34}.

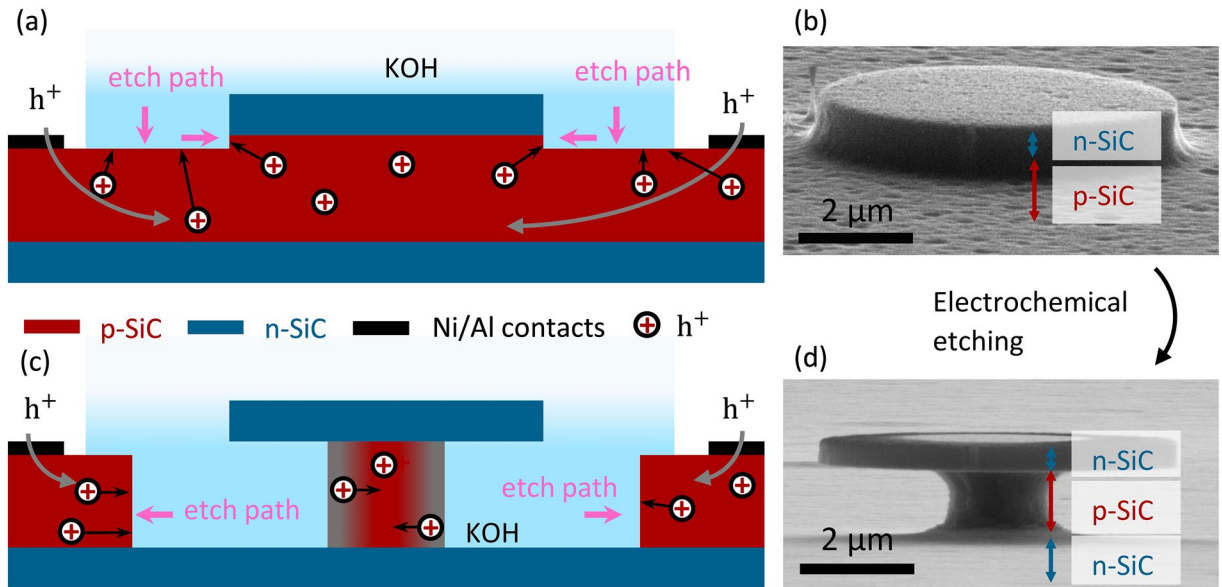


Figure 4. Electrochemical etching using dopant-defined layers. **(a,b)** Before ECE, areas to be removed are defined by lithography and gas etching slightly into the p-layer. Positive charge carriers (h^+), required for ECE, are supplied via Ni/Al ohmic contacts. Applying anodic voltages results in (energy) band bending of the semiconductor, holes accumulate at the p-SiC/KOH interface and promote etching. **(c, d)** ECE removes the p-SiC layer. The etching is stopped vertically by the n-SiC layer; the lateral etching is stopped as soon as the remaining p-island is electrically unconnected. Without any applied potential, the p-SiC/KOH interface depletes of holes (due to band bending, grey area). **(b,d)** SEM micrographs, scale-bar: 2 μm .

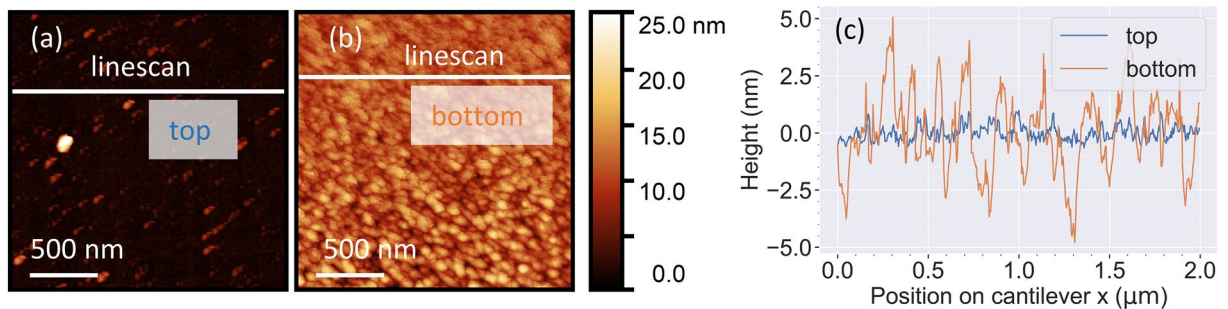


Figure 5. Surface characterization after ECE. AFM measurements on a cantilever (top and bottom surfaces). Statistical evaluation yields roughnesses of $\text{rms}_{\text{top}} = 1.46 \text{ nm}$ and $\text{rms}_{\text{bottom}} = 2.48 \text{ nm}$. The scale-bar refers to 500 nm. **(b)** Height profiles referring to the lines indicated in **(a)**.

entire temperature range with completely processed devices like cantilever structures or membranes. They were exposed to high temperature steps in Ar atmosphere (900 mbar) for 30 min and subsequently investigated with SEM (see Fig. 6a–d) and AFM (Fig. 6e). The shape of the cantilevers is maintained at least up to 1550°C. Beyond this temperature, as can be seen in Fig. 6d a visible re-arrangement occurs. It is most obvious at the lower edge, where a discontinuity has been created. Also in the lower and upper left corners, an additional faceted transition is formed, following crystalline directions. Remarkably, below 1550°C, our cantilevers provide an excellent shape stability. An analysis of the upper surface profile shows very little effect up to 1200°C. In the temperature range of 1275°C to 1350°C, pronounced terraces are formed and step bunching occurs (4° miscut) with typical step heights of the order of 10 nm, beyond 1550°C approaching towards 25 nm.

From the contrast in the SEM micrographs, the characteristic pattern of the initiation of graphene growth becomes apparent, which forms a homogenous coverage when annealing the sample at 1700°C¹¹. This is more than an interesting detail: epitaxial graphene provides an atomically smooth surface termination that is inert as long as oxygen plasma is avoided.

In conclusion, we present a versatile electrochemical fabrication route for generating high-quality monolithic 3D devices in SiC. The shape of the 3D structure is defined by doping profiles. The surface quality can be enhanced by high temperature annealing. While in this study, we limited ourselves to homogenous p-type layers and homogeneous n-type top layers, much more refined 3D shaping is possible. Such 3D devices, monolithically carved out of monocrystalline SiC wafers, pave the way to implement mechanical and optical monolithic devices with excellent surface properties on the SiC platform. Together with the already available electrical semiconductor

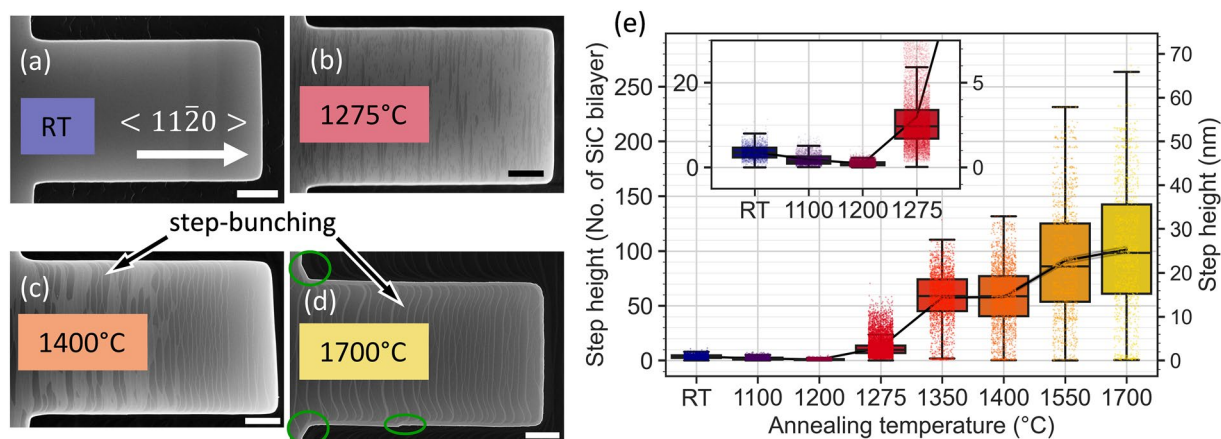


Figure 6. Cantilever shape evolution during high-temperature annealing. **(a–d)** SEM micrographs of the very same cantilever after step-wise annealing at selected temperatures. Faceted reconfigurations are highlighted in green. Scale-bar: 2 μm . **(e)** AFM line-scans were performed in the $\langle 11\bar{2}0 \rangle$ direction. The plot shows the analysis of the step height of this annealed cantilever as a function of annealing temperature. The SiC step height significantly increases for annealing temperatures above 1275°C. The step height is additionally given in units of SiC bilayer, 0.25 nm. The insert is a zoom emphasizing the low-temperature range.

functionalities, graphene electronics and spin-physics in SiC a rich toolbox can be established, unifying quantum and classical technologies on the very same chip (Supplementary Information).

Data availability

The data that support the findings of this study is available in an open-access repository: <https://doi.org/10.22000/1722>.

Received: 29 June 2023; Accepted: 26 October 2023

Published online: 04 November 2023

References

1. She, X., Huang, A. Q., Lucia, O. & Ozpineci, B. Review of silicon carbide power devices and their applications. *IEEE Trans. Industr. Electron.* **64**, 8193–8205 (2017).
2. Lukin, D. M. *et al.* 4H-silicon-carbide-on-insulator for integrated quantum and nonlinear photonics. *Nat. Photon.* **14**(5), 330–334 (2020).
3. Ghaffari, S. *et al.* Quantum limit of quality factor in silicon micro and nano mechanical resonators. *Sci. Rep.* **3**, 1–7 (2013).
4. Lukin, D. M., Guidry, M. A. & Vučković, J. Integrated quantum photonics with silicon carbide: Challenges and prospects. *PRX Quantum* **1**, 020102 (2020).
5. Crook, A. L. *et al.* Purcell enhancement of a single silicon carbide color center with coherent spin control. *Nano Lett.* **20**(5), 3427–3434 (2020).
6. Sato, H., Abe, M., Shoji, I., Suda, J. & Kondo, T. Accurate measurements of second-order nonlinear optical coefficients of 6H and 4H silicon carbide. *JOSA B* **26**, 1892–1896 (2009).
7. De Leonardis, F., Soref, R. A. & Passaro, V. Dispersion of nonresonant third-order nonlinearities in Silicon Carbide. *Sci. Rep.* **7**, 1–12 (2017).
8. Lukin, D. M., *et al.* Two-emitter multimode cavity quantum electrodynamics in thin-film silicon carbide photonics. *Physical Review X* **13**(1), 011005 (2023).
9. Hamelin, B., Yang, J., Daruwalla, A., Wen, H. & Ayazi, F. Monocrystalline silicon carbide disk resonators on phononic crystals with ultra-low dissipation bulk acoustic wave modes. *Sci. Rep.* **9**, 1–8 (2019).
10. Heinrich, S. M. & Dufour, I. Fundamental Theory of Resonant MEMS Devices, in Resonant MEMS, John Wiley & Sons, Ltd, p. 1–28 (2015).
11. Emtsev, K. V. *et al.* Towards wafer-size graphene layers by atmospheric pressure graphitization of silicon carbide. *Nat. Mater.* **8**(3), 203–207 (2009).
12. Rühl, M., Ott, C., Götzinger, S., Krieger, M. & Weber, H. B. Controlled generation of intrinsic near-infrared color centers in 4H-SiC via proton irradiation and annealing. *Appl. Phys. Lett.* **113**, 122102 (2018).
13. Boyd, G. D., Coldren, L. A. & Storz, F. G. Directional reactive ion etching at oblique angles. *Appl. Phys. Lett.* **36**, 583–585 (1980).
14. Takahashi, S. *et al.* Direct creation of three-dimensional photonic crystals by a top-down approach. *Nat. Mater.* **8**, 721 (2009).
15. Frye, C. D., *et al.* High temperature isotropic and anisotropic etching of silicon carbide using forming gas. *J. Vacuum Sci. Technol. A* **39** (2021).
16. Zhuang, D. & Edgar, J. H. Wet etching of GaN, AlN, and SiC: a review. *Mater. Sci. Eng. R. Rep.* **48**, 1–46 (2005).
17. Van Dorp, D. H., Weyher, J. L. & Kelly, J. J. Anodic etching of SiC in alkaline solutions. *J. Micromech. Microeng.* **17**, S50 (2007).
18. Van Dorp, D. H. & Kelly, J. J. Photoelectrochemistry of 4H-SiC in KOH solutions. *J. Electroanal. Chem.* **599**, 260–266 (2007).
19. Van Dorp, D. H. Etching of wide-bandgap chemically resistant semiconductors: An electrochemical study, Utrecht University, (2008).
20. Rysy, S., Sadowski, H. & Helbig, R. Electrochemical etching of silicon carbide. *J. Solid State Electrochem.* **3**, 437–445 (1999).
21. Shor, J. S., Kurtz, A. D., Grimberg, I., Weiss, B. Z. & Osgood, R. M. Dopant-selective etch stops in 6H and 3C SiC. *J. Appl. Phys.* **81**, 1546–1551 (1997).
22. Zhao, F., Islam, M. M. & Huang, C.-F. Photoelectrochemical etching to fabricate single-crystal SiC MEMS for harsh environments. *Mater. Lett.* **65**, 409–412 (2011).
23. Adachi, K. *et al.* Single-crystalline 4H-SiC micro cantilevers with a high quality factor. *Sens. Actuators A Phys.* **197**, 122–125 (2013).

24. Shor, J. S. & Kurtz, A. D. Photoelectrochemical etching of 6 H-SiC. *J. Electrochem. Soc.* **141**, 778 (1994).
25. Leitgeb, M. *et al.* Stacked layers of different porosity in 4H SiC substrates applying a photoelectrochemical approach. *J. Electrochem. Soc.* **164**, E337 (2017).
26. Cook, L. M. Chemical processes in glass polishing. *J. Non-Cryst. Solids* **120**, 152–171 (1990).
27. Glembocki, O. J., Palik, E. D., De Guel, G. R. & Kendall, D. L. Hydration model for the molarity dependence of the etch rate of Si in aqueous alkali hydroxides. *J. Electrochem. Soc.* **138**, 1055 (1991).
28. Leitgeb, M. *et al.* Communication—current oscillations in photoelectrochemical etching of monocrystalline 4h silicon carbide. *ECSS J. Solid State Sci. Technol.* **10**, 073003 (2021).
29. Föll, H., Leisner, M., Cojocaru, A. & Carstensen, J. Self-organization phenomena at semiconductor electrodes. *Electrochimica Acta* **55**, 327–339 (2009).
30. Hochreiter, A. & Weber, H. B., Research data for the manuscript: Electrochemical etching strategy for shaping monolithic 3D structures from 4H-SiC wafers. <https://doi.org/10.22000/1722> (2023).
31. Negoro, Y., Katsumoto, K., Kimoto, T. & Matsunami, H. Electronic behaviors of high-dose phosphorus-ion implanted 4H-SiC (0001). *J. Appl. Phys.* **96**, 224–228 (2004).
32. Weiße, J., Hauck, M., Krieger, M., Bauer, A. J. & Erlbacher, T. Aluminum acceptor activation and charge compensation in implanted *p*-type 4H-SiC. *AIP Adv.* **9**, 055308 (2019).
33. Weisse J., *et al.* Analysis of compensation effects in aluminum-implanted 4H-SiC devices. *Materials Science Forum* (2018).
34. Rambach, M., Bauer, A. J. & Ryssel, H. Electrical and topographical characterization of aluminum implanted layers in 4H silicon carbide. *Phys. Status Solidi b.* **245**(7), 1315–1326 (2008).
35. Zangoie, S. & Arwin, H. Surface, pore morphology, and optical properties of porous 4H-SiC. *J. Electrochem. Soc.* **148**, G297 (2001).
36. Shor, J. S., Osgood, R. M. & Kurtz, A. D. Photoelectrochemical conductivity selective etch stops for SiC. *Appl. Phys. Lett.* **60**, 1001–1003 (1992).
37. Shin, M. W. & Song, J. G. Study on the photoelectrochemical etching process of semiconducting 6H-SiC wafer. *Mater. Sci. Eng. B* **95**, 191–194 (2002).
38. Powers, J. M. & Somorjai, G. A. The surface oxidation of alpha-silicon carbide by O₂ from 300 to 1373 K. *Surf. Sci.* **244**, 39–50 (1991).
39. Pierucci, D. *et al.* Atomic and electronic structure of trilayer graphene/SiC (0001): Evidence of strong dependence on stacking sequence and charge transfer. *Sci. Rep.* **6**, 33487 (2016).

Acknowledgements

Support from Patrik Schmuki and Matthias A. Popp in early stages of this work is acknowledged. Discussions with Sabine Maier about the AFM data evaluation and representation are acknowledged. Support and conduction of ion implantations by Willi Rösch are acknowledged. We further acknowledge financial support by German Research Foundation (DFG, QuCoLiMa, SFB/TRR 306, Project No. 429529648), project B03.

Author contributions

A.H. developed the etching strategy, fabricated samples and conducted the measurements. F.G. conducted the annealing experiments. M.N.M. fabricated the membrane. M.K. contributed his experience in SiC processing. H.B.W. conceived the experiment. The manuscript was written by A.H. and H.B.W. All authors discussed the results and contributed to the final manuscript.

Funding

Open Access funding enabled and organized by Projekt DEAL.

Competing interests

The authors declare no competing interests.

Additional information

Supplementary Information The online version contains supplementary material available at <https://doi.org/10.1038/s41598-023-46110-2>.

Correspondence and requests for materials should be addressed to H.B.W.

Reprints and permissions information is available at www.nature.com/reprints.

Publisher's note Springer Nature remains neutral with regard to jurisdictional claims in published maps and institutional affiliations.



Open Access This article is licensed under a Creative Commons Attribution 4.0 International License, which permits use, sharing, adaptation, distribution and reproduction in any medium or format, as long as you give appropriate credit to the original author(s) and the source, provide a link to the Creative Commons licence, and indicate if changes were made. The images or other third party material in this article are included in the article's Creative Commons licence, unless indicated otherwise in a credit line to the material. If material is not included in the article's Creative Commons licence and your intended use is not permitted by statutory regulation or exceeds the permitted use, you will need to obtain permission directly from the copyright holder. To view a copy of this licence, visit <http://creativecommons.org/licenses/by/4.0/>.

© The Author(s) 2023